Oral Presentation

TSME International Conference on Mechanical Engineering
13-16 December 2016

TSF0026

Effect of Computational Box Sizes on Opposition Control at Moderate-High Friction Reynolds Number Turbulent Channel of $Re_\tau = 934$

Vasin Satthavisut[1,*], Vejapong Juttijudata[1] and Arpiruk Hokpunna[2]

[1] Department of Aerospace Engineering, Faculty of Engineering, Kasetsart University, Bangkok 10900, Thailand
[2] Department of Mechanical Engineering, Faculty of Engineering, Chiang Mai University, Chiang Mai 50200, Thailand
[*] Corresponding Author: v.satthavisut@gmail.com, Tel: +66 (0) 2 627 2772

Abstract

The objective of this study is to investigate the effect of the computational box sizes on the large scale structures as well as the turbulent statistics and the amount of drag reduction in manipulated channels. The study is based on Large-Eddy Simulation of the turbulent channel flows. A large computational box size up to $8\pi h \times 3\pi h$ in streamwise and spanwise, is chosen to capture a very large scale motion. An opposition control was used and applied at a lower wall. It is found that no significant difference was observed between the small and large channels. For the Re_τ tested here, the computational box size of $2\pi h \times \pi h$ in streamwise and spanwise, is sufficiently large enough to produce a reliable prediction of the amount of drag reduction and the one-point turbulent statistics which are comparable with the large box.

Keywords*:* Drag reduction, High Reynolds number, Large-Eddy Simulation, Opposition control

1. Introduction

Since the turbulent skin-friction drag contributes a large portion of the total drag on commercial aircraft, cargo ships, high-speed trains, and other streamlined vehicles, any reduction in the skin-friction drag on these vehicles can result in a huge saving of fuel consumptions, operating costs, emissions, and protecting the global environment. Therefore, the successful flow control strategies to reduce the skin-friction drag can lead to substantial benefits, especially for the transportation industry. Many numerical and experimental studies have been performed to seek for the effective and practical control strategies for the drag reduction.

The conventional active control strategies for the turbulent drag reduction, using sensors and actuators distributed on the wall to suppress the near-wall coherent structures and to reduce drag, work effectively at the low Reynolds number [1]. However, as the Reynolds number increases, the effectiveness of the conventional active control strategies decreases as a result of the contribution of the coherent structures further away from the wall becoming more important [2,3], despite the channel sizes in the studies are small and can only capture the large-scale motion (LSM) which is in the order of half-channel height, h. Recent studies [e.g. 4,5] reveal that a strong interaction of the near-wall coherent structures and the large-scale motion (LSM) and the very large-scale motion (VLSM) further away from the wall, which is in the order of ten times of the half-channel height, $10h$, is responsible for the turbulence production and can only be captured in a large channel. The presence of the VLSM in a large channel may further reduce the effectiveness of the conventional active control strategies and required new control strategies to reduce the drag of the turbulent channel at a high Reynolds flow in the large channel containing a wide range of scales of the motion including the VLSM.

The goal of this study is to investigate an effect of computational box sizes on the VLSM as well as the turbulent statistics and the amount of drag reduction in manipulated channels by means of the opposition control. In the light of the result obtained, new control strategies can be developed for the high Reynolds number flow in a large (and more realistic) channel.

2. Theory and Related Works

2.1 Opposition control

Opposition control is a simple feedback control strategy that introduces a control to counteract the near-wall streamwise vortical structures. As illustrated by Fig. 1, the impose wall blowing and suction are in an opposition to the wall-normal velocity measured at a detection (sensing) plane located at a distance z_d from the wall,

$$w(x,y,0;t) = -w(x,y,z_d;t) \qquad (1)$$

where x, y, and z are the streamwise, spanwise, and wall-normal coordinates, respectively, and t is time. The velocity component in u, v and w are in the x-, y-, and z-directions, respectively.

This control can leads up to 25% drag reduction at low Reynolds Re_τ = 180 (based on wall friction velocity) [1]. However, as the Reynolds number increases, the effectiveness of drag reduction drop from 26% at Re_τ = 100 to 19% at Re_τ = 720 [2]. They also observed that the optimal detection planes move closer to the wall as the Reynolds number increased, i.e. from $z_d^+ = 15$ at $Re_\tau = 180$ to $z_d^+ = 12.5$ at $Re_\tau = 720$.

TSF0026

2.2 Large scale structures in high Reynolds number wall turbulent

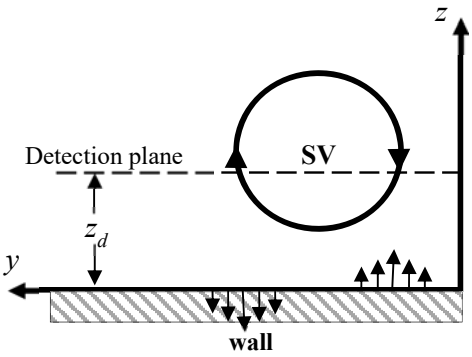

Fig. 1 Schematic diagram of opposition control.

Recent high Reynolds studies [4,7] show the evidence that there are large-scale structures in the outer layer, in the form of long regions of streamwise velocity fluctuation. This finding was enriched by [8] suggesting that the large scales structures exist at all Reynolds number but they become important and contribute more in term of their energy containing and interaction with smaller scales near the wall when increasing the Reynolds number.

In general, the large-scale motions (LSMs) have a streamwise scale up to 2~3h while the very large-scale motions (VLSMs) have a streamwise scale larger than 3h. For example, the largest scale of 10h was observed in the turbulent channel flow experiment at Re_τ = 960 [7].

However, most previous studies on an active turbulence control are conducted in small channel sizes and can only capture the LSMs. In order to capture the VLSMs and study their effect to an effectiveness of the conventional opposition control properly, a large channel box, up to 8πh and 3πh in the streamwise (x) and the spanwise (y) directions [5], is chosen in this study. At this box size, the largest scales up to 12h that can be captured properly which is large enough to contain the scale of 10h according to the experiment finding.

3. Computational Details

The study is based on the Large-Eddy Simulation (LES) of a fully-developed turbulent channel flow with the WALE sub-grid scale (SGS) model [9] at a moderate high friction Reynolds number of $Re_\tau = u_\tau h/\nu$ = 934, based on a wall friction velocity of unmanipulated channel, u_τ and a half-channel height, h. A compact fourth-order finite volume on the staggered grids is used for solving the incompressible Navier-Stokes equations. The time advancement is done by an explicit third-order Runge-Kutta method. The flow is periodic in the streamwise and spanwise directions, while a no-slip boundary condition is imposed on the walls. The pressure gradient is kept constant throughout the study. The code was well-validated in [10]. The flow geometry and the coordinate system used are shown in Fig. 2.

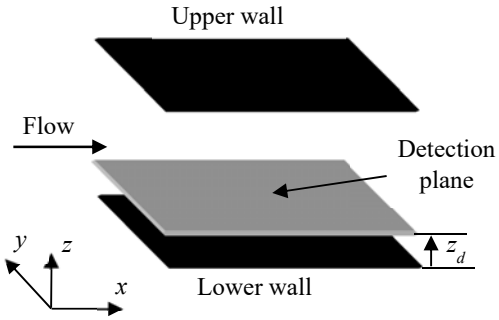

Fig. 2 Flow geometry and coordinate system used in channel flows.

To examine the effect of the large-scale structures on the drag reduction of an active turbulence control, three different computational box sizes are considered. The first one, a small channel of $[L_x, L_y] = [2\pi h, \pi h]$, the second one, a medium channel of $[L_x, L_y] = [4\pi h, 2\pi h]$, and the last one, a large channel of $[L_x, L_y] = [8\pi h, 3\pi h]$ in the streamwise and spanwise directions (hereafter called 2PI, 4PI, and 8PI, respectively). All box sizes are using a constant grid spacing of $[\Delta_x^+, \Delta_y^+, \Delta_z^+] = [46, 23, 1\sim16.2]$ based on the wall unit of an unmanipulated channel. A summary of the computational parameters and gird resolutions are presented in Table. 1. In the LES, the superscript $^+$ denotes a non-dimensional quantity scaled by the kinematic viscosity, ν and the friction velocity of the unmanipulated channel, $u_\tau = (\tau_w/\rho)^{1/2}$, where τ_w is the mean wall-shear stress and ρ is the fluid density. For example, $z^+ = zu_\tau/\nu$ and $u^+ = U/u_\tau$. The time step size of 0.004 h/u_b was used and leads to CFL less than 0.4 in all simulations. The flows were allowed to develop until reaching the statically steady state, before the applied control started.

An opposition control is chosen as a based control strategy. Actuators are distributed on the wall in order to actively suppress the near-wall coherent structures while sensing plane locates in the viscous layer of the flow. In this study, the opposition control will be applied at the lower wall only. By the extrapolation of their results [2], z_d^+ = 11.5 is chosen for an optimal sensing plane location of the near-wall control for the Re_τ studied here. Due to given wall-normal discretization, the actual sensing plane located at z_d^+ = 11.1; the closest plane to z_d^+ = 11.5. The control is implemented on all channel sizes.

4. Results and Discussion

4.1 LES of unmanipulated channel (No control)

In order to examine the effect of the VLSM on the turbulence statistics of no control, three different box sizes were used and tested at the same Re_τ. All simulations data were collected at the same total amount of time (t) of ~840 h/u_b, correspond to 33 through flows

TSF0026

Table. 1 Computational box sizes and grid resolutions of unmanipulated and manipulated channels.

Case	Re_τ	L_x	L_y	N_x	N_y	N_z	$N_{total}\times10^6$	Δx^+	Δy^+	Δz^+_{min}	Δz^+_{max}
2PI (Small box)	934	$2\pi h$	πh	128	128	128	2.1	45.82	22.91	0.9854	16.21
4PI (Medium box)	934	$4\pi h$	$2\pi h$	256	256	128	8.4	45.82	22.91	0.9854	16.21
8PI (Large box)	934	$8\pi h$	$3\pi h$	512	384	128	25.2	45.82	22.91	0.9854	16.21

Table. 2 Mean flow variables of unmanipulated channels after the flow reach stationary state.

Case	$Re_{\tau,eff}$	u_τ	u_b	τ_w	C_f	%Error	total time	tu_b/L_xh
2PI, No control	937.96	5.122E-02	0.984	2.599E-03	5.366E-03	5.41%	840.8	131.8
4PI, No control	938.12	5.123E-02	0.986	2.605E-03	5.356E-03	5.21%	840.8	66.0
8PI, No control	937.70	5.121E-02	0.985	2.599E-03	5.354E-03	5.17%	838.0	32.9
Ref. DNS data	934	4.539E-02	0.900	2.062E-03	5.091E-03	-	-	-

in 8PI case (the large box), which is long enough to ensure the flow reaching statically steady state and allowing sufficient time for the VLSM to form properly. A summary of the mean flow variables of the no control case is shown in Table. 2. The reference case is the DNS data [5] with the same computational box size of 8PI and similar Re_τ studied here. The skin-friction coefficient (C_f) from current study is compared to DNS from [5], defined as,

$$C_f = \tau_w / (\frac{1}{2}\rho u_b^2) \quad (2)$$

$$u_b = \frac{1}{2h}\int_0^{2h} U(z)dz \quad (3)$$

where τ_w is the mean wall shear stress, ρ is the fluid density which equal to 1 in this study and u_b is a bulk velocity across the channel.

The results show the Error of C_f (compared to [5]) in range between 5.17–5.41%. The lowest error is in the 8PI case while the largest error is in the 2PI case. Only 0.24% difference of the C_f can be observed in the largest and the smallest boxes while the total number of grid points are 12-times more. It appears that the effect of the VLSM is not so important and has very small effect on the skin-friction coefficient at the Re_τ tested here. In other words, the small box size of 2PI is sufficient to produce a good C_f which is comparable with the large box size.

Fig. 3 and 4 show the mean velocity profile and the rms velocities of unmanipulated channel compared against the DNS data. In overall, the mean velocity profiles of all simulations are in a good agreement with DNS data. The first grid point is located at $z^+ \sim 1$ and 5 total points are in the region of $0 < z^+ < 10$. The data collapsed well in the region of viscous wall layer ($1 < z^+ < 20$). The results are slightly under predicted of mean profile after $z^+ > 20$ up to center of the channel. This is caused by an over prediction of the wall shear stress resulting in higher of u_τ and Re_τ. This implied that the flow in the LES moves slightly slower than the DNS due to more friction at wall. Similarly, the rms velocities of all simulations are in good agreement with

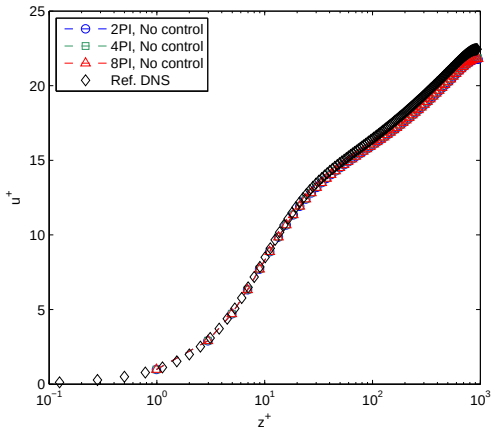

Fig. 3 Mean velocity profile of unmanipulated channel in three different box sizes compared with DNS data of large channel in wall coordinates [5].

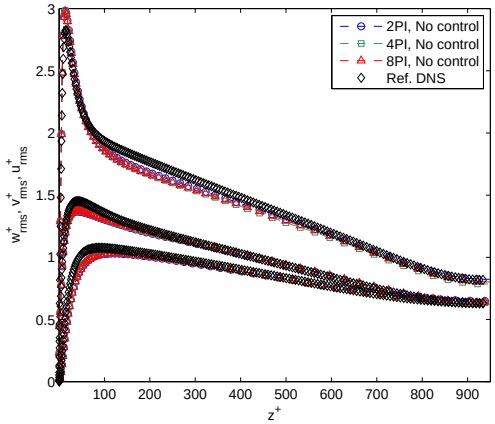

Fig. 4 rms velocity profiles of unmanipulated channel in three different box sizes compared with DNS data of large channel in wall coordinates [5].

DNS data. The peak of u_{rms}^+ is slightly over predicted by 5.3% while the location is shift toward the wall, from 15 to 13.4 wall units. The trend of u_{rms}^+ is over predicted

up to z^+= 50, and then under predicted up to center of the channel. The v_{rms}^+ and w_{rms}^+ are slightly under predicted up to z^+ = 300, beyond that, the data are collapse well with the DNS. However, the u_{rms}^+ of the 2PI case is slightly over predicted than the others. This may caused by the effects of periodic condition that feedback the VLSM back into the box. So the VLSM will be seen as the infinite long and leads to more artificial turbulence levels.

4.2 LES of manipulated channel (Opposition control at lower wall)

Since the simulation is based on a constant mean pressure gradient (CPG), the successful control strategy will leads to a reduction in the local wall shear stress and an increase of bulk flow velocity (the flow can move more easily due to less friction). However, in this study, the opposition control is applied at a lower wall only (instead of both walls), resulting in an asymmetric of the mean velocity profile. The location of maximum velocity is shifted from the center of channel toward the controlled side i.e. the lower wall. This behavior is depicted in Fig. 5(a). In this case, the lower portion of the channel up to the location of maximum velocity will be treated as the Turbulent Boundary Layer flow (TBL). Therefore, the formulation to compute a local skin friction coefficient (c_f) for TBL case can be applied;

$$c_{f,lower} = \tau_{w,lower} / (\frac{1}{2} \rho u_{\max}^2) \qquad (4)$$

where u_{max} is the maximum mean velocity of the manipulated channel and a new variable, h' is an effective turbulent boundary layer thickness (a distance between the lower wall up to the maximum velocity location). The h' can be found by plotting the wall distance in the global coordinates, z/h (x-axis) against the total shear stress (y-axis), then finding the x-intercept (the location where the value of total shear stress equal to zero). Once the h' is known, we can obtain the mean velocity that corresponds to h' by using a linear interpolation – found that at $z = h$', the velocity is maximum i.e. $u(h') = u_{max}$; it is reasonable to approximate u_∞ in effective TBL to u_{max} in Eq. (4). In this study, all simulations give an identical h' which is equal to 0.9. Fig. 5(b) shows a plot of the wall distance against total shear stress of manipulated channel in the global coordinates.

A summary of the mean flow parameters and the *Drag Reduction* of manipulated channel in various box sizes is shown in Table. 3. The minimum total time of ~250 h/u_b was used for collecting the statistics of all controlled cases. Note that c_f in Table. 3 is defined by Eq. (4); it is different from C_f in Table. 2 defined by Eq. (2).

Similar to the study of an unmanipulated channel, all controlled cases give almost identical results of the %*DR* which is equal to 20.7% for the Re_τ studied here. Only 0.02% difference is observed between 2PI and 8PI cases. The control reduces the wall shear stress, resulting in increasing of a bulk velocity and a maximum velocity and finally, the reduction of the local skin-friction coefficient.

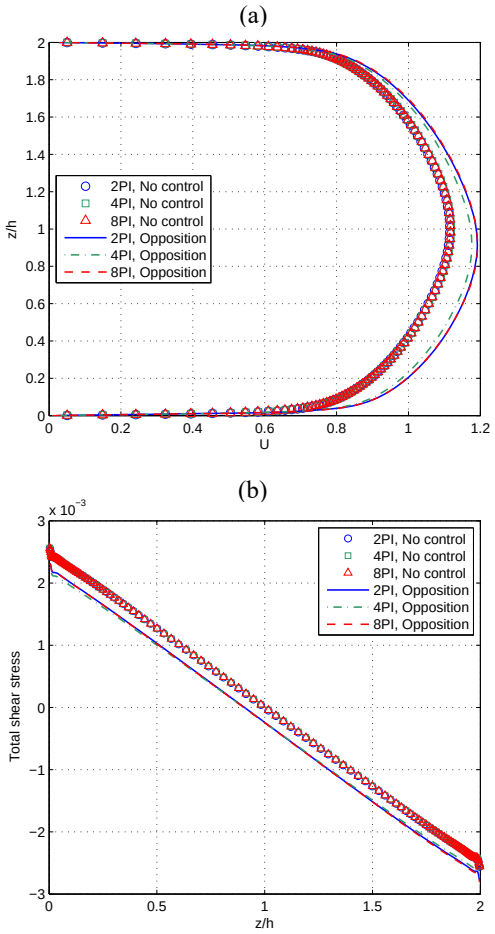

Fig. 5 LES statistics of manipulated channel in various box sizes. (a) mean velocity profile in global coordinates. The flow is from left to right while the opposition control was applied at a lower wall, $z/h = 0$ and (b) a wall distance across the channel against the total shear stress in the global coordinates. The x-intercept was shifted to the left hand side when the control applied: unfilled marker, no control; filled marker, opposition controlled with the sensing plane location at $z_d^+ = 11.1$ (actual value).

Moreover, the accuracy of our drag reduction can be improved by refining the mesh in a spanwise direction. The mesh refinement might be the right choice to be considered rather than putting more effort/computing power on increasing the size of the computational domain. Since it is known that the resolution in the spanwise direction plays an important role in predicting the accurate drag reduction [3]. The gird size should be fine enough to capture the near wall streamwise vortices precisely, which is known as the main source of turbulence. In addition, our results demonstrate that there is no significant effect of the VLSM on both unmanipulated and manipulated channels can be observed. In short, at this Re_τ tested

TSF0026

Table. 3 Mean flow variables and drag reduction (%*DR*) of manipulated channel in various box sizes.

Case	$Re_{\tau,eff}$	u_τ	u_b	u_{max}	h	$\tau_{w,\,lower}$	c_f	%*DR*
No control								
2PI, No control	937.96	5.122E-02	0.984	1.115	1.000	2.599E-03	4.180E-03	-
4PI, No control	938.12	5.123E-02	0.986	1.119	1.000	2.605E-03	4.163E-03	-
8PI, No control	937.70	5.121E-02	0.985	1.117	1.000	2.599E-03	4.169E-03	-
Opposition control (at lower wall)					***h'***			
2PI, Opposition	819.34	4.940E-02	1.057	1.191	0.906	2.352E-03	3.314E-03	20.72%
4PI, Opposition	806.08	4.873E-02	1.043	1.176	0.903	2.292E-03	3.313E-03	20.41%
8PI, Opposition	815.87	4.935E-02	1.058	1.192	0.903	2.348E-03	3.304E-03	20.74%

here, the box size of 2PI is sufficiently large enough for the study of flow control which is able to reproduce the amount of drag reduction that is comparable with the large box size.

The comparison of the LES turbulent statistics between unmanipulated and manipulated channels from all sizes of box are shown in Fig. 6 and 7. In general, all controlled cases give an increase in the mean velocity and a reduction in the rms velocity except for the 2PI case which has the u_{rms}^+ from unmanipulated case slightly over than the manipulated case in the region of $100 < z^+ < 750$. This may be a result of a reduction of h' in the controlled case. As in the small channel, the VLSM structure will be seen as the infinite long throughout the box leading to more artificial in turbulence levels of the streamwise direction. That's why the u_{rms}^+ in a small channel is not collapsed well with the larger channels.

For the mean velocity profile, it is clearly seen in Fig. 6(a) that the profile was shifted in an upward direction, implied that the flow in the manipulated channel moves faster than in the unmanipulated channel due to less friction. The slope of mean velocity remains unchanged, up to $z^+ \sim 9$, beyond that point up to the center of the channel, the profile of the controlled case has been shifted in an upward direction. This upward shift is a result of an increase in viscous sub-layer thickness due to less friction and wall friction velocity.

Similarity are also observed in the rms velocity as shown in Fig. 6(b). All turbulence intensities are decreasing, obviously on the peak value of u_{rms}^+ and in the region $100 < z^+ < 850$ of the streamwise rms component. The peak of u_{rms}^+ was reduced by 5.34%. While the location of the peak is shifted outward from $z^+ = 13.41$ to 17.75. Another key feature on the opposition control is that the control will establish a virtual wall (or slip wall). This wall is defined as a location where the local value of w_{rms}^+ equal to zero or minimum while the other components, u_{rms}^+ and v_{rms}^+ are non-zero at this location. The virtual wall is located between the actual wall and the detection plan location. This feature also links to the drag reduction mechanism. Since the concept of the opposition control is to inject wall-normal velocity to counteract and reduce the wall-normal momentum transport of the near-wall coherent structures to the wall. Once the streamwise vortices

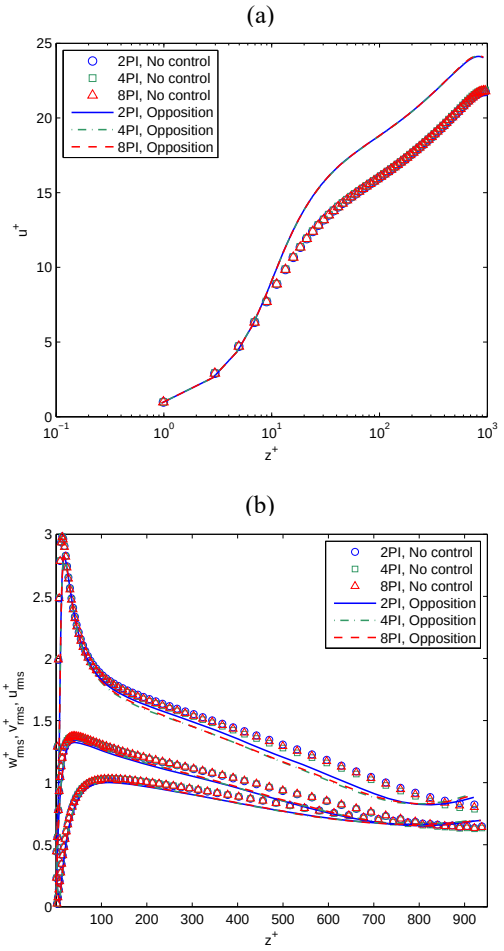

Fig. 6 LES statistics of manipulated channel in three different box sizes. The variables are normalized the local friction velocity. (a) mean velocity profile in wall coordinates and (b) rms velocity profiles in wall coordinates; For legend, see caption Fig. 5.

were suppressed, leading to the reduction of steak formation and finally, interrupting and deferring the near-wall regeneration cycles. This phenomenon is depicted in Fig. 7(a). In this study, the virtual wall was established at $z^+ \sim 8$, while the w_{rms}^+ intensity was

reduced from 0.205 to 0.049. As a result of the reduction in u_{rms}^+ and w_{rms}^+ intensities, the reduction of Reynolds stress was also observed in Fig. 7(b).

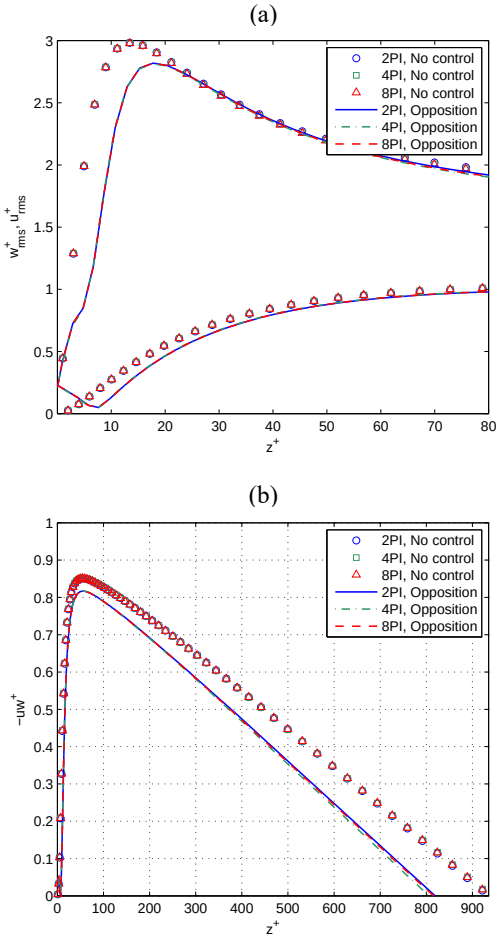

Fig. 7 LES statistics of manipulated channel in various box sizes. The variables are normalized by the local friction velocity. (a) a zoom-in of streamwise and wall-normal rms velocities in wall coordinates, from the lower wall up to $z^+ = 80$ and (b) Reynolds shear stress of the lower channel in wall coordinates, from the lower wall up to center of the channel. For legend, see caption Fig. 5.

In summary, at the Re_τ = 934 tested here, the domain size of 2PI is sufficient for the study of flow control for drag reduction. With this box size, reliable one-point turbulent statistics and the amount of drag reduction, which are comparable with the large box size, can be obtained.

4.3 Visualization of the velocity fields

To gain more understanding about the effect of computational box size and drag reduction mechanism, the instantaneous velocity field were visualized and examined in this section. Fig. 8 – 10 show contours of streamwise velocity fluctuation of unmanipulated and manipulated channels of 2PI and 8PI cases. Two wall-parallel planes located at $z^+ = 13.4$ and $z = 0.11h$ as well as a cross-flow plane were considered here.

For the unmanipulated channel, both box sizes demonstrate the feature of near-wall streaky structures, Fig. 8(a) – (b). The low-speed region or streak ($u'/u_\tau < 0$, blue color) in the form of thin and elongated structures as well as the high-speed region ($u'/u_\tau > 0$, red color) in the form of wider and shorter structures than the streak. The similar coherent streaky structures also observed in the region further away from the wall, Fig. 9(a) – (b). The most clearly observation is the length of streak is longer than $8h$ (VLSM). Resulting in, the VLSM in the 2PI case will be seen as the infinite long (due to periodic condition) leads to more artificial turbulence intensity in the streamwise direction. This is depicted by the darker contour level in Fig. 10(a) – (b).

For the manipulated channel, both box sizes present the similar results. The near-wall streaky structures are become more shorter and less frequent, Fig. 8(c) – (d). The contour level also soften corresponds to the reduction of rms velocity as depicted in Fig. 6(b) and 7(a). Further spectral analysis will be conducted to quantify the change of streak size. Following with a region further away from the wall investigation (Fig. 9), the results compare to the unmanipulated channel are almost no different. Then, a cross-flow plane comparison (Fig. 10); at the lower wall (which was controlled), the weaken streaks observed (see lighter contour). Also, the LSM in 2PI case seems to be a little stronger close to center of the channel.

5. Conclusion

A LES of moderate-high Reynolds number turbulent channel flows have been performed to study the effect of computational box sizes on the large scale structures in both unmanipulated and manipulated channels. A large computational box size up to 8PI ($8\pi h \times 3\pi h$) was used in this study. The opposition control is chosen and applied at the lower wall. The results show less than 0.5% difference in the skin-friction coefficient in unmanipulated channel while 0.02% difference in the drag reduction was observed in manipulated channel. The one-point turbulent statistics are similar on both small and large channels. Therefore, the computation box size of 2PI ($2\pi h \times \pi h$) is sufficiently large enough to produce the amount of drag reduction and the one-point statistics which is comparable with the large box size for the Re_τ = 934 tested here.

6. Acknowledgement

The authors gratefully acknowledged the HPC services from the WATA Cluster, Faculty of Engineering, Kasetsart University and the OCEAN Cluster, Large Scale Simulation Research Laboratory, NECTEC for providing the computing resources for this project.

TSF0026

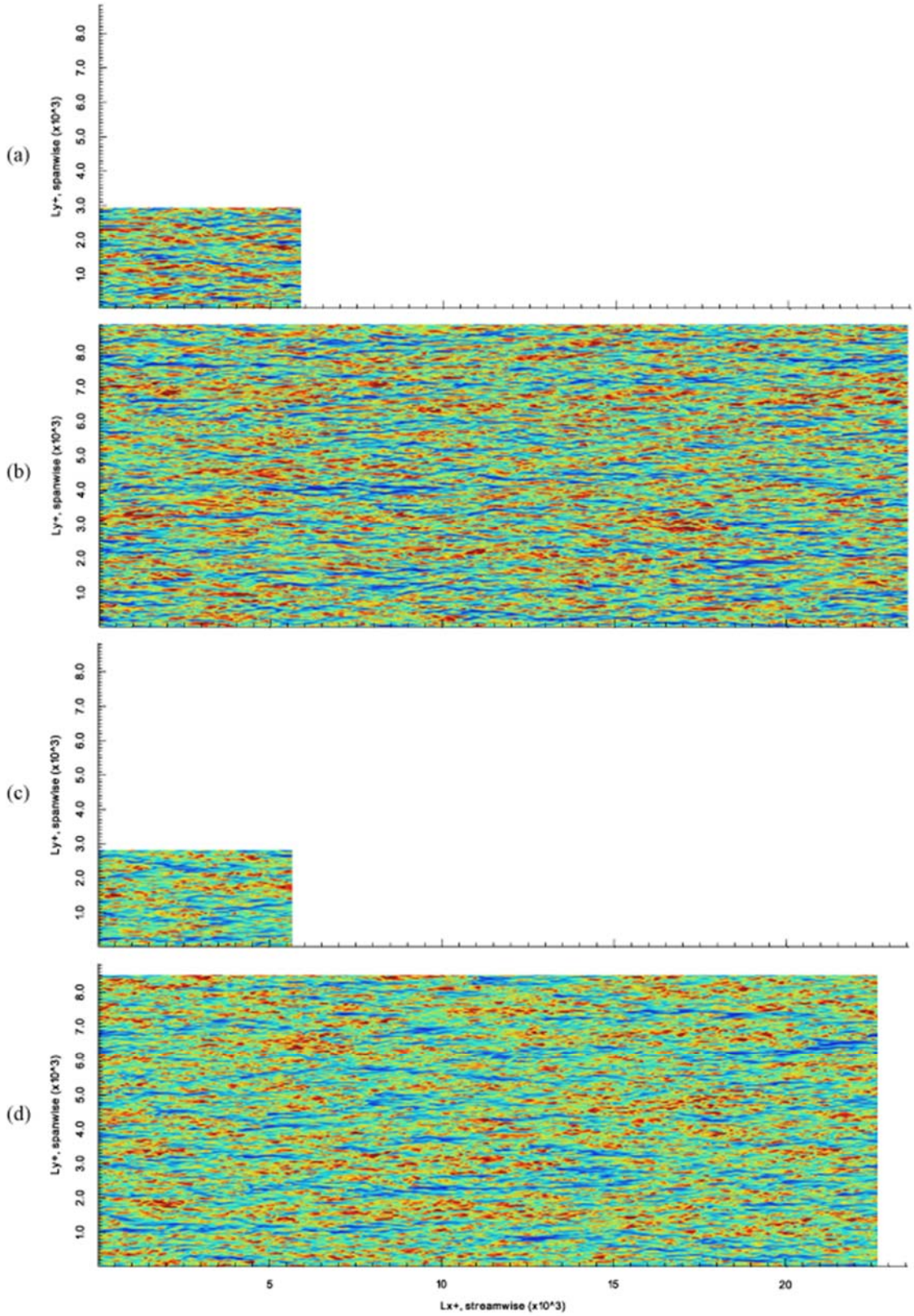

Fig. 8 Instantaneous streamwise velocity fluctuation in a x-y plane at $z^+ \sim 13$. (a) No control of 2PI; (b) No control of 8PI; (c) Opposition control of 2PI; (d) Opposition control of 8PI; The streamwise & spanwise lengths are in wall units. Contour levels are shown for $-6 \leq u'/u_\tau \leq 6$.

Fig. 9 Instantaneous streamwise velocity fluctuation in a x-y plane at $z \sim 0.11h$. (a) No control of 2PI; (b) No control of 8PI; (c) Opposition control of 2PI; (d) Opposition control of 8PI; The streamwise & spanwise lengths are in outer units. Contour levels are shown for $-6 \leq u'/u_\tau \leq 6$.

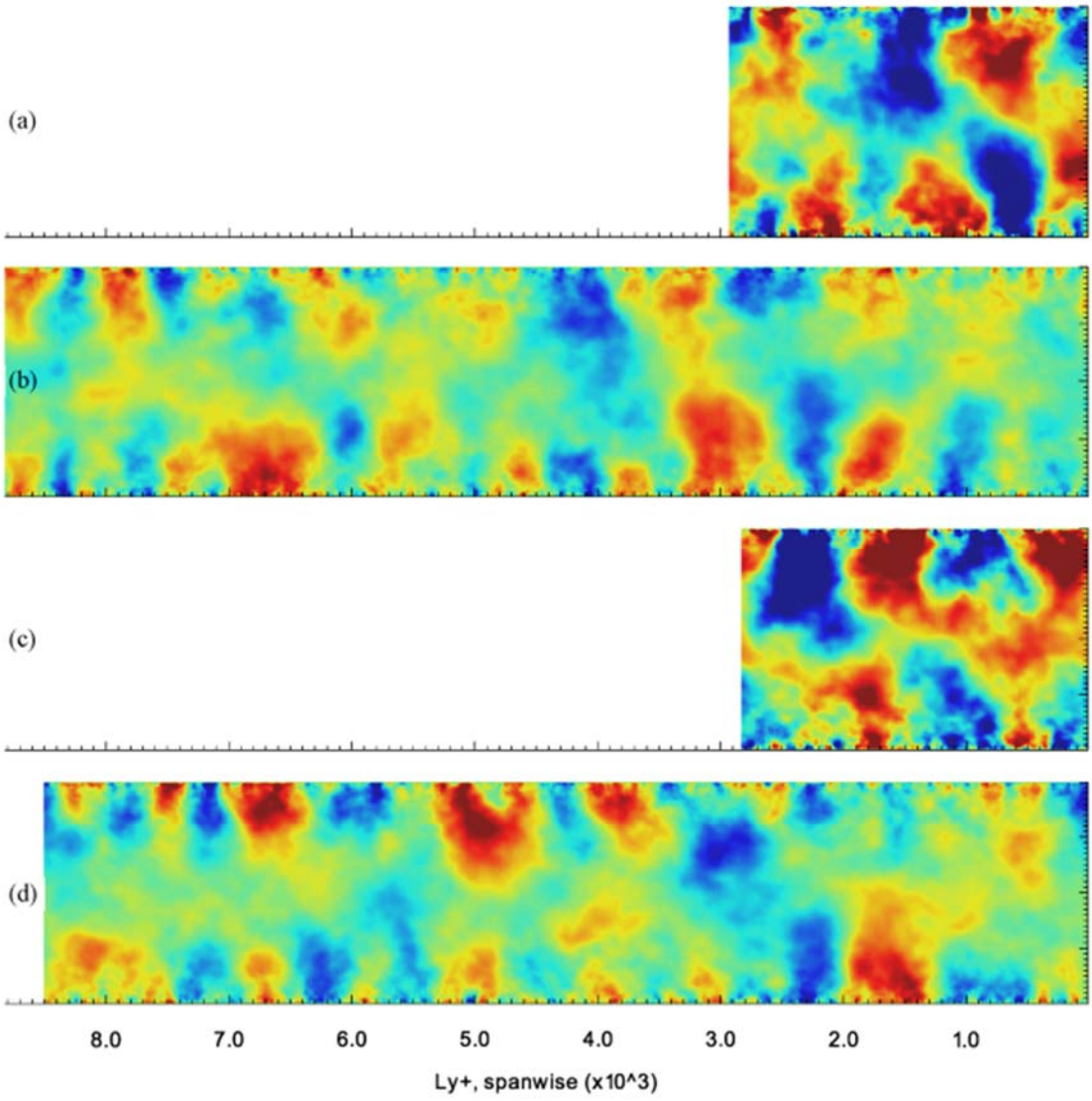

Fig. 10 Instantaneous streamwise velocity fluctuation in the cross-flow plane, *y*-*z* plane. (a) No control of 2PI case; (b) No control of 8PI case; (c) Opposition control of 2PI case; (d) Opposition control of 8PI case; The velocity fields are averaged in streamwise direction. The spanwise lengths are in wall units. Contour levels are shown for -0.06 (blue) ≤ u' ≤ 0.06 (red).

7. References

[1] Choi, H., Moin, P. and Kim, J. (1994). Active turbulence control for drag reduction in wall-bounded flows, *Journal of Fluid Mechanics*, vol.262, October 1994, pp. 75 – 110.

[2] Iwamoto, K., Suzuki, Y. and Kasagi, N. (2002). Reynolds number effect on wall turbulence: toward effective feedback control, *International Journal of Heat and Fluid Flow*, vol.23(5), October 2002, pp. 678 – 689.

[3] Chang, Y., Collis, S. S. and Ramakrishnan, S. (2002). Viscous effects in control of near-wall turbulence, *Physics of Fluids*, vol.14(11), October 2002, pp. 4069 – 4080.

[4] Kim, K.C. and Adrian, R.J. (1999). Very large-scale motion in the outer layer, *Physics of Fluids*, vol.11(2), February 1999, pp. 417 – 422.

[5] Del Álamo, J. C., Jiménez, J., Zandonade, P. and Moser, R. D. (2004). Scaling of the energy spectra of turbulent channels, *Journal of Fluid Mechanics*, vol.500, January 2004, pp. 135 – 144.

[6] Fukagata, K., Iwamoto, K. and Kasagi, N. (2002). Contribution of Reynolds stress distribution to the skin friction in wall-bounded flows, *Physics of Fluids*, vol.14(11), November 2002, pp. L73 – L76.

[7] Balakumar, B. J. and Adrian, R.J. (2007). Large-and very-large-scale motions in channel and boundary-layer flows, *Philosophical Transactions of the Royal Society A*, vol.365(1852), March 2007, pp. 665 – 681.

TSF0026

[8] Smits, A.J., McKeon, B.J. and Marusic, I. (2011). High-Reynolds number wall turbulence, *Annual Review of Fluid Mechanics*, vol.43, January 2011, pp. 353 – 375.

[9] Nicoud, F. and Ducros, F. (1999). Subgrid-scale stress modelling based on the square of the velocity gradient tensor, *Flow, Turbulence and Combustion*, vol.62(3), September 1999, pp. 183 – 200.

[10] Hokpunna, A. and Manhart, M. (2010). Compact fourth-order finite volume method for numerical solutions of Navier–Stokes equations on staggered grids, *Journal of Computational Physics*, vol.229(20), October 2010, pp. 7545 – 7570.

[11] Juttijudata, V. (2006). Turbulent drag reduction – A direct numerical simulation approach, paper presented in *the 10th Annual National Symposium on Computational Science and Engineering (ANSCSE)*, Chiang Mai, Thailand.

[12] Chung, Y.M. and Talha, T. (2011). Effectiveness of active flow control for turbulent skin friction drag reduction, *Physics of Fluids*, vol.23(2), February 2011, pp. 025102 1 – 10.

[13] Stroh, A., Frohnapfel, B., Schlatter, P. and Hasegawa, Y. (2015). A comparison of opposition control in turbulent boundary layer and turbulent channel flow. *Physics of Fluids*, vol.27(7), July 2015, pp. 075101 1 – 14.